Flow Measurement and Instrumentation 94 (2023) 102479

Contents lists available at ScienceDirect

Flow Measurement and Instrumentation

journal homepage: www.elsevier.com/locate/flowmeasinst

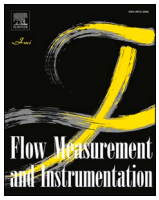

Effect of probe size on phase-detection probe measurements of air-water flow properties in hydraulic jumps

Rui Shi [a,b], Davide Wüthrich [c,*], Hubert Chanson [d]

[a] Rio Tinto, Perth, Australia
[b] Formerly at School of Civil Engineering, The University of Queensland, Brisbane QLD 4072, Australia
[c] Department of Hydraulic Engineering, Delft University of Technology, Delft, the Netherlands
[d] School of Civil Engineering, The University of Queensland, Brisbane, QLD 4072, Australia

ARTICLE INFO

Keywords:
Hydraulic jump
Phase detection conductivity probes
Air–water flow properties
Physical modelling

ABSTRACT

This experimental study investigated the air-water flow properties and bubble characteristics in hydraulic jumps with Froude numbers $Fr_1 = 2.4$ and 6.3, using four dual-tip phase detection probes with sensor sizes from 0.25 mm to 0.64 mm. The hydraulic jumps were characterized by a fully breaking roller with substantial air entrainment and turbulent two-phase flow patterns. The measurements encompassed distributions of void fraction, bubble count rate, interfacial velocity and bubble clustering properties and the data sets were consistent with previous studies. The comparison of the different probes showed a small impact of the tested sensor sizes on the air-water flow properties, in terms of the trends, magnitude and maximum values. Some differences were observed in terms of the bubble count rate, with the larger probes detecting a lesser number of bubbles. The trend was further confirmed through a comparison with the data set of Chanson and Brattberg (2000) [10] with a smaller probe sensor size ($Ø_1 = 0.025$ mm), in which the maxima of bubble count rates were almost twice that of the present dataset for identical flow conditions. The present results confirm that the traditional signal processing techniques can be used for relatively small probe sizes, although different approaches might be needed for larger probes which cannot detect sub-millimetric bubbles. Overall, the findings should facilitate the development of sturdier phase-detection needle probes and help breaching the gap between laboratory and prototype.

1. Introduction

Air-water flows are commonly observed in both natural and built environments [1,2]. To investigate these flows, intrusive phase-detection probes were introduced to quantify their key two-phase properties, interfacial velocities and turbulent characteristics [3,4,5]. Investigations with intrusive phase-detections probes measure either the difference in conductivity between air and water (conductivity probes), or the difference in light refraction (optical fibre probes). Several studies focused on air-water flow properties in hydraulic jumps because of their suitability as energy dissipators in hydraulic structures. Latest investigations employed dual-tip phase-detection conductivity probes [6,7,8,9,10], whilst fewer works used single-tip probes [11] and most recently, an array of phase detection probes [12].

Phase-detection conductivity needle probes consist of an inner electrode insulated from an outer electrode within a tube of small dimensions, typically less than 1 mm. Prototype measurements of air-water flows are rare because hindered by the fragility of probe sensors and the development of thicker and sturdier instruments has been a challenge for decades. Hohermuth et al. [13] reported practical challenges restraining the use of conductivity probes in prototype measurement. Yet, successful air-water flow measurements were performed in flows with interfacial velocities up to 18 m/s using a needle with 0.2 mm inner sensor size [14], up to 22 m/s with 1 mm sensor size [15], and up to 38 m/s with an outer diameter of 0.6 mm [13]. In hydraulic jumps, prototype measures were conducted using conductivity probes (inner electrode 0.1 mm, outer electrode 0.8 mm), sustaining inflow velocities of 5.9–8.6 m/s [16,17]. A more comprehensive summary of studies on air-water flow properties using various probe size can be found in Shi et al. [18]. These studies demonstrated that the construction of mechanically resistant probes is an achievable goal, but a larger sensor size enhances the probe's intrusiveness and might alter the acquired phase-detection signal. Previous studies have shown that the size of the inner conductor has an influence on the air-water flow properties,

* Corresponding author.
E-mail address: d.wuthrich@tudelft.nl (D. Wüthrich).

https://doi.org/10.1016/j.flowmeasinst.2023.102479
Received 28 June 2023; Received in revised form 13 October 2023; Accepted 21 October 2023
Available online 30 October 2023

including bubble size characteristics and interfacial area data [15,3,19,20]; . The influence of probe's inner sensor diameter $Ø_1$ on the air-water flow measurements in plunging jets and stepped chutes was briefly discussed by Refs. [21,20,22,23]. Reference [24] suggested the outer diameter $Ø_2$ to be a key factor affecting the sensor intrusiveness, hinting that an increasing tube diameter reduced the chance of detecting small particles, although the needle shape must also be considered. For hydraulic jumps, Tang et al. [25] provided a comparison between laboratory and prototype measurements ($Ø_2$ = 3 mm), introducing a modified signal processing method to extract reliable air-water flow properties from the thick-tip probe outputs.

While it is acknowledged that all intrusive phase-detection probes affect the measured signal, previous results seem to show a limited impact of the probe sensor size on the void fraction and interfacial velocity data. On the other hand, some larger differences were observed in terms of bubble count rate and bubble size characteristics [26,20]. Despite a practical relevance, some general knowledge on the effect of sensor size on the air-water flow properties remains limited. For this reason, the objective of this study is to provide an assessment of the effect of sensor size in air-water flow measurements in hydraulic jumps with two Froude numbers and relatively high Reynolds numbers, using several double-tip phase-detection probes with different sensor sizes. With larger sensors becoming more widely used in field measurements, these results are critical for the development of sturdier phase-detection conductivity probes that will support future research in breaching the gap between laboratory and prototype.

2. Experimental approach

2.1. Experimental set-up and instrumentations

A new series of experiments was performed in a large-size facility at the University of Queensland, Australia. A hydraulic jump was induced in a horizontal channel with a 3.2 m long, 0.5 m wide and 0.4 m deep rectangular section, where x, y and z represented the longitudinal, transverse and vertical coordinates, respectively (Fig. 1). Water was initially issued from an upstream head tank equipped with flow straighteners and a rounded undershoot gate, inducing a horizontal and contraction-less impinging flow. The downstream test section was built with a smooth HDPE bed and glass sidewalls. The longitudinal position of the roller toe x_{toe} was controlled through an adjustable overshoot vertical gate located at channel downstream end. The water discharge was measured using a Venturi flowmeter (precision ±2%) and up/down-stream water depths were measured with a pointer gauge with an accuracy of ±0.5 mm.

The air-water properties were investigated using four double-tip phase-detection conductivity probes manufactured at the University of Queensland. Each probe had two identical needle sensors with a longitudinal separation distance Δx, parallel mounted with a transverse separation distance Δy (Figs. 1 and 2). The sensor had an inner conductor filament with a diameter $Ø_1$, covered with coasting material with a diameter $Ø_{coat}$, isolating the conductor from an outer needle made of stainless steel with a diameter $Ø_2$. In the present study, the sensor size referred to the inner conductor diameter $Ø_1$. An array of two phase-detection probes was used to record the data instantaneously on the channel centreline (Fig. 2). The detailed dimensions of the phase-detection probes are listed in Table 1, including the probe information for two previous studies, since these data are used for comparison [7,10]. Following a number of previous studies (*e.g.* Refs. [25,10,12]), the phase-detection probes were sampled with an acquisition frequency of 20 kHz per sensor for 45s.

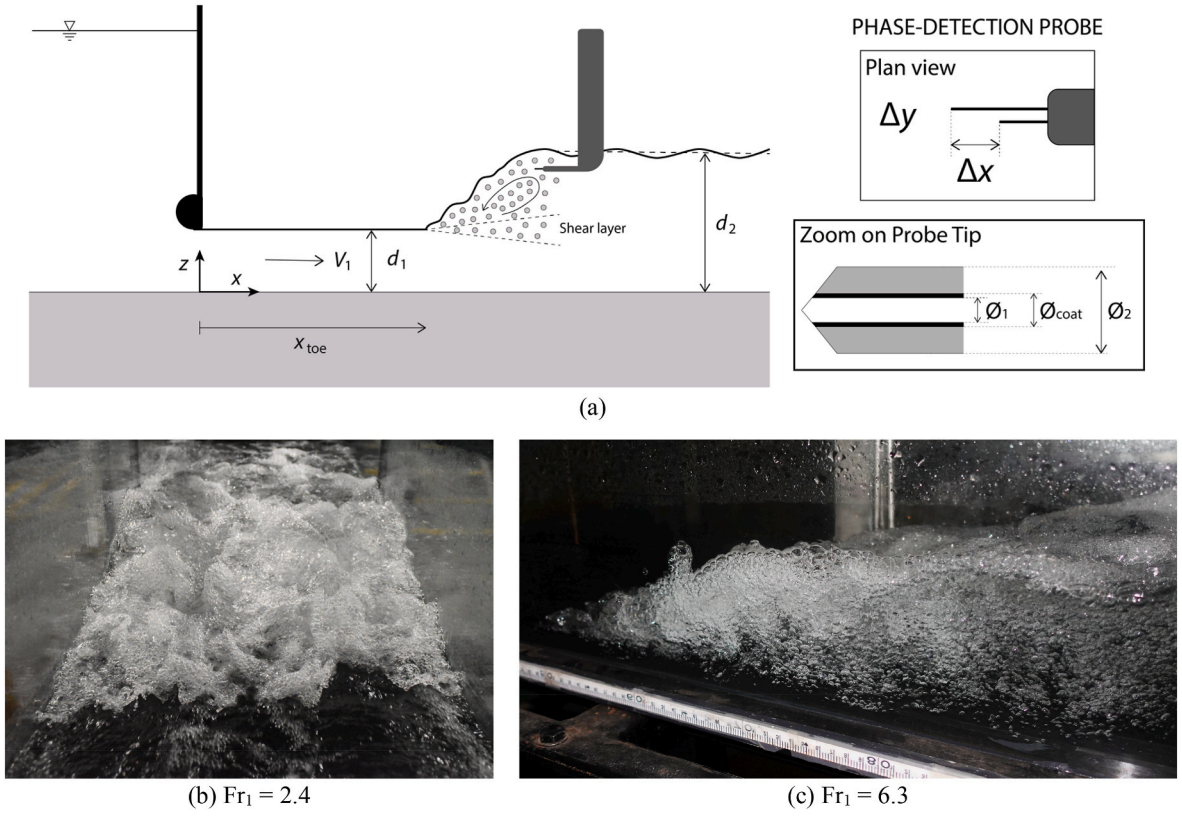

Fig. 1. (a) Sketch of experimental facility and instrumentation, including details of the conductivity probes; (b) Front view of the hydraulic jump with $Fr_1 = 2.4$; (c) Side view of the hydraulic jump roller for $Fr_1 = 6.3$; the support of the phase-detection probe is seen above the roller. Both pictures were taken with a relatively high shutter speed.

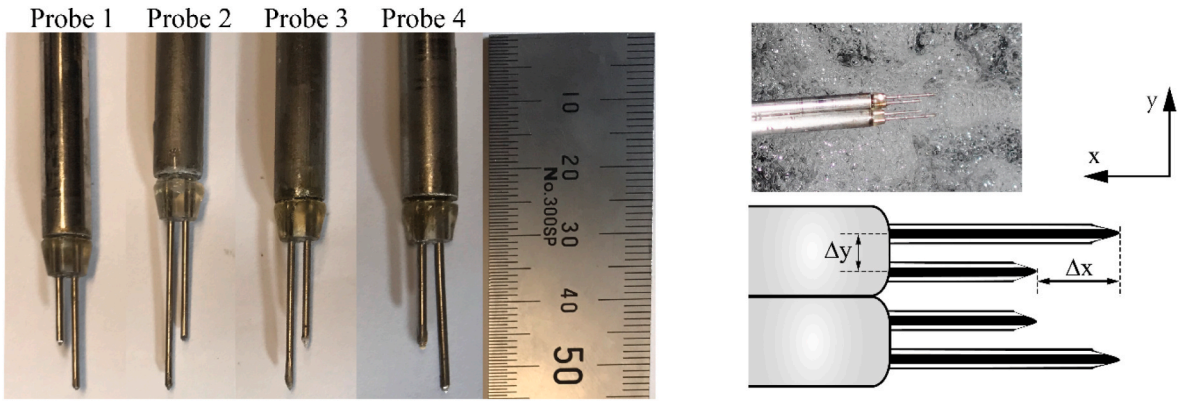

Fig. 2. Photos and sketches of the conductivity probes used in the present study: (left) photo of Probe 1 to 4; (right) sketch and picture of the probe array.

Table 1
Summary of flow conditions investigated in the present study and double-tip phase-detection conductivity probes used at the University of Queensland.

References	Fr_1	Re	d_1 [m]	V_1 [m/s]	Probe No.	$Ø_1$ [mm]	$Ø_2$ [mm]	$Ø_{coat}$ [mm]	Δx [mm]	Δy [mm]	Conductor material	Manufacturer of conductor
Chanson and Brattberg [7]	6.3	$3.3{\cdot}10^4$	0.014	2.3	6	0.025	0.20	0.043	8.00	1.33	Platinum	Goodfellow, UK
Wuthrich et al. [10]	2.4	$1.9{\cdot}10^5$	0.084	2.2	5	0.25	0.80	0.298	5.10	1.80	Silver	Goodfellow, UK
Present study	2.4	$1.9{\cdot}10^5$	0.084	2.2	1	0.25(*)	1.00	0.298	7.5	2.47	Silver	Goodfellow, UK
	6.3	$3.3{\cdot}10^4$	0.014	2.3	2	0.25(*)	1.00	0.330	7.8	2.20	Silver	SDR Scientific, UK
					3	0.38	1.10	0.480	7.0	2.22	Silver	SDR Scientific, UK
					4	0.64	1.30	0.760	6.8	3.23	Silver	SDR Scientific, UK

(*) Note that the inner conductors of Probe 1 and 2 had the same size $Ø_1$, but came from different manufacturers.

2.2. Flow conditions

The hydraulic jumps are described using their inflow Froude number $Fr_1 = V_1/(g{\cdot}d_1)^{0.5}$, where V_1 is the initial flow velocity, d_1 the initial flow depth and g the gravitational constant. In addition, the Reynolds number is defined as $Re = \rho V_1 d_1/\mu$, where ρ is the water density and μ the dynamic viscosity. As detailed in Table 1, this work focuses on two flow conditions: $Fr_1 = 2.4$ in line with Wthrich et al. [10] and $Fr_1 = 6.3$ for comparison with the data set of Chanson and Brattberg [7] who used a dual-tip phase-detection probe with a smaller tip sensor diameter ($Ø_1 = 0.025$ mm and $Ø_2 = 0.2$ mm). This approach therefore provides a data comparison for six different phase-detection probe sensor sizes ranging from 25 μm to 640 μm (Table 1).

The Froude number was shown to highly influence the air-water properties in hydraulic jumps, especially the maximum void fraction and bubble count rate in the developing shear layer [27]. Thus, in the present study the air-water flow properties were measured at vertical profiles corresponding to four different longitudinal locations $(x\text{-}x_{toe})/d_1 = 1.19$, 3.57, 7.14 and 14.29, where x is the longitudinal distance from the inlet, d_1 the initial flow depth and, x_{toe} is the time-averaged position of the jump. Herein $x_{toe} = 1.3$ m for $Fr_1 = 2.4$ as in Ref. [10]; and $x_{toe} = 0.5$ m for $Fr_1 = 6.3$ as per [7].

2.3. Signal processing

Based on the different values of their electrical resistance/conductivity, the needle-shaped sensors simultaneously detected whether the tip was located in air or water [28,29]. The raw signal was post-processed using a single threshold technique set at 50% of the voltage difference between air and water [3,7], thus assigning an instantaneous void fraction value of 1 for air and of 0 for water. The time-averaged void fraction C was defined as the average time spent in air relative to the total time. The bubble count rate F was defined as the number of air bubbles or water droplets per second, calculated as half of the total number of air-water and water-air interfaces over the total sampling duration. The air-water interfacial velocity V was obtained through a cross-correlation technique as $V = \Delta x/T$, where Δx was the longitudinal distance between the two tips and T was the time lag corresponding to the maximum cross-correlation coefficient between leading and trailing tip signals [15,28]. The advection of large-scale coherent structures leads to non-random regrouping of air bubbles, namely the clustering [30]. In the present study, a near-wake criterion was used to define the one-dimensional bubble clustering [31,32]. That is, a cluster forms when two bubbles travel one after another with an interval time smaller than the passage time of the leading bubble. The longitudinal clustering properties were investigated, in terms of clustering count rate F_{clu} defined as the number of clusters per second, average cluster size N_{clu} defined as the average number of bubbles per cluster, and cluster proportion P_{clu} defined as the ratio of the number of bubbles in clusters to total number of bubbles. Following Wang and Chanson [33] the bubble clustering was studied for $0 < C < 0.3$, and droplet clustering for $0.7 < C < 1.0$.

3. Data analysis

The data analyses focused on the main air-water flow properties, including void fraction (Section 3.1), bubble count rate (Section 3.2), interfacial velocities (Section 3.3), bubble clustering properties (Section 3.4) and bubble chord time statistics (Section 3.5), based on signal processing described in Section 2.3.

3.1. Void fraction

The vertical distributions of time-averaged void fraction are presented in Figs. 3a and 4a for $Fr_1 = 2.4$ and 6.3, respectively, at different longitudinal locations behind the jump and for various phase-detection probes. For both flow conditions, the data exhibited a typical bell-shape in the developing shear layer, where the profile tended to flatten with increasing longitudinal distance. This region was followed by a monotonically increasing distribution when approaching the free surface.

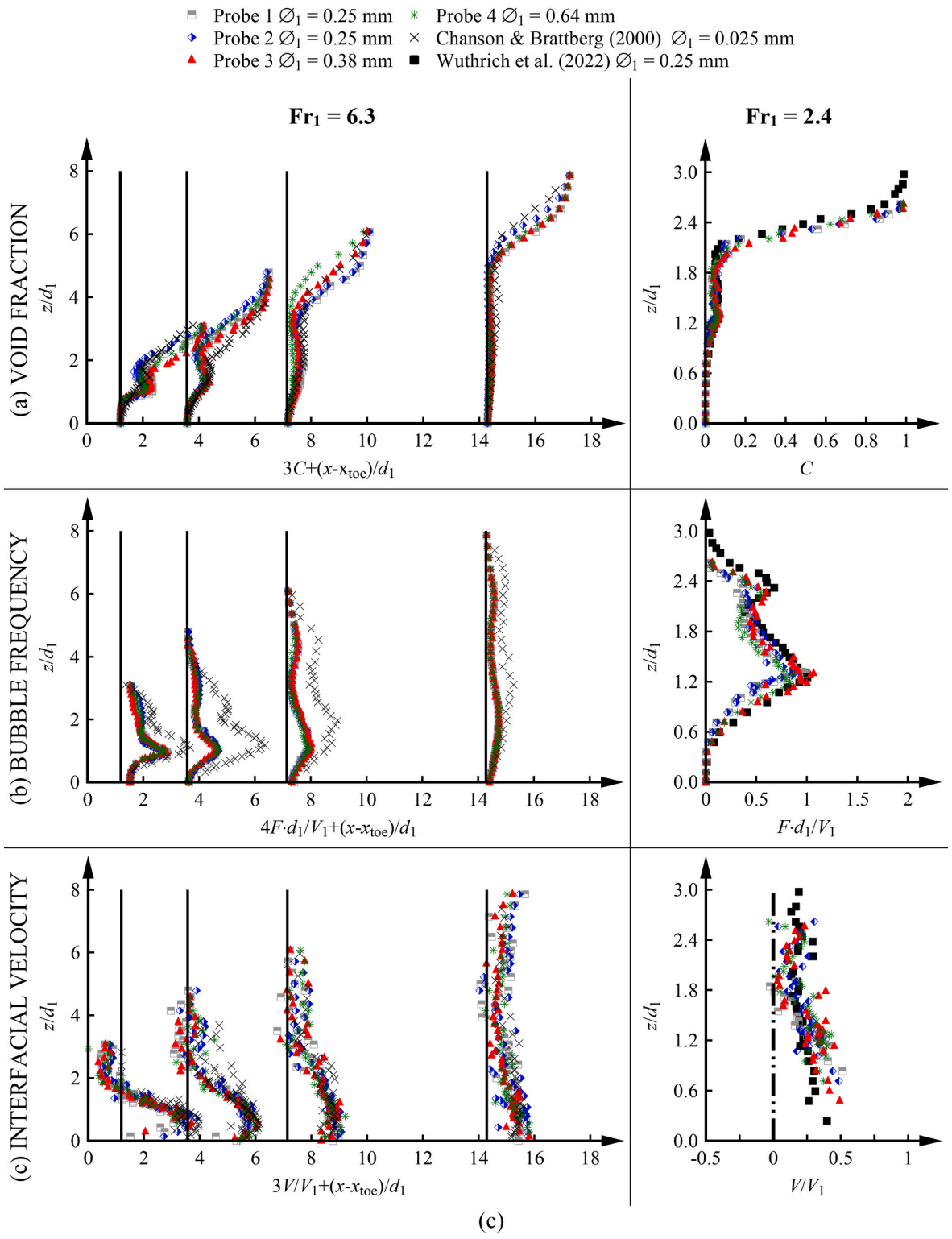

Fig. 3. Air-water properties measured with different probes in a hydraulic jump with: (left) $Fr_1 = 6.3$; and (right) $Fr_1 = 2.4$. Properties include: (a) void fraction C; (b) bubble count rate F; (c) time-averaged interfacial velocity V. Data for $Fr_1 = 6.3$ were compared to Chanson and Brattberg [7]; while data for $Fr_1 = 2.4$ was compared to Wuthrich et al. [10] at $(x - x_{toe})/d_1 = 3.57$. Legend applies to all figures.

Overall, the present findings were consistent with data from several previous studies, including [7,34,9]. A good agreement can be seen for all void fraction profiles recorded with the five probes, with some differences close to the upper free-surface, where the presence of large-size air pockets might have an influence on the air-water signal. Yet, the current data suggested that the range of inner sensor diameters tested in the present study had a minimal impact on the void fractions, in line with Tang et al. [25].

Maximum values of the void fraction in the shear layer (C_{max}) are characterized by a rapid decay downstream of the roller toe [*i.e.* increasing values of $(x - x_{toe})/d_1$], likely due to an intensive air diffusion process near the impingement point. While this decay is well-known in

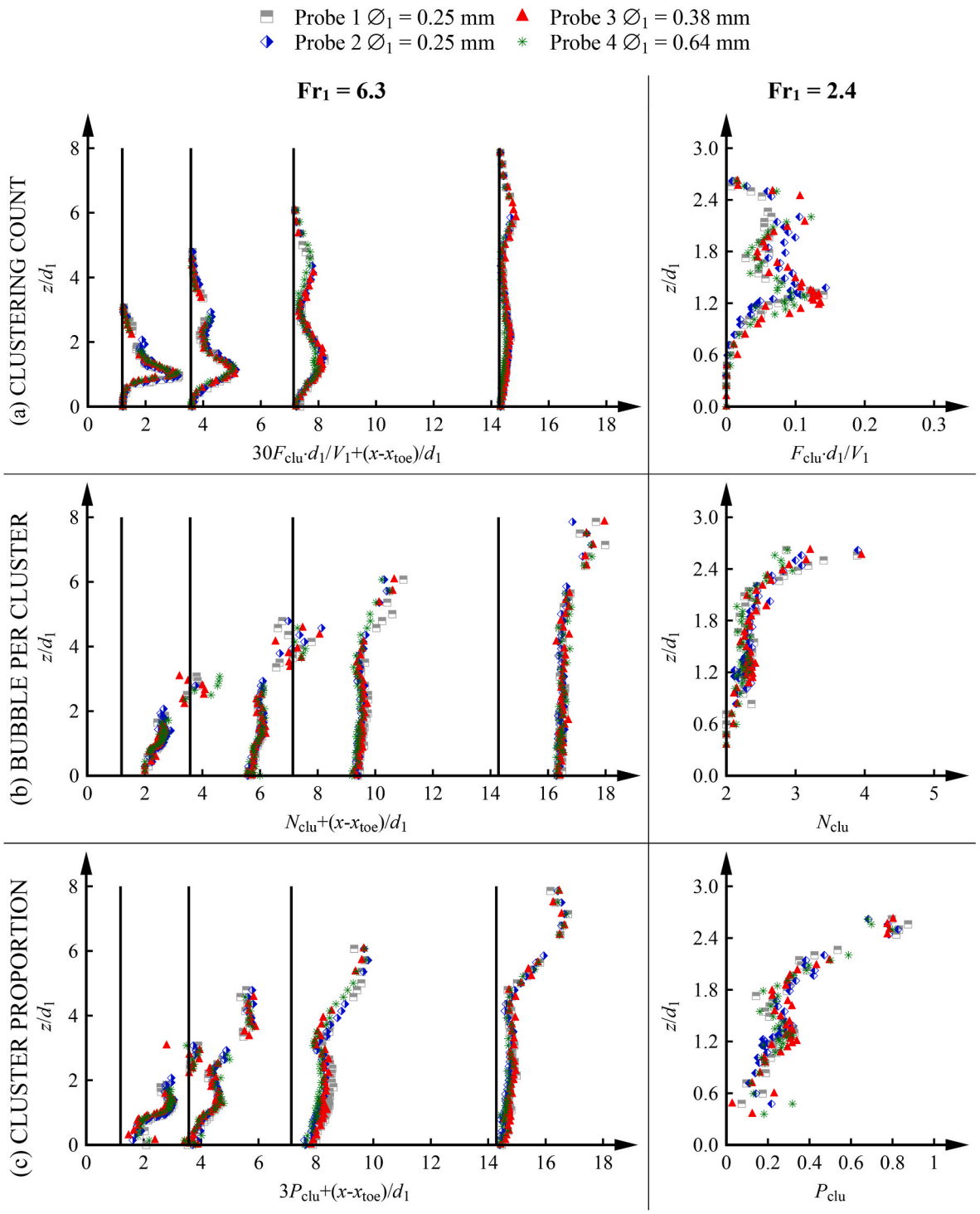

Fig. 4. Air-water properties measured with different probes in a hydraulic jump with: (left) $Fr_1 = 6.3$; and (right) $Fr_1 = 2.4$. Properties include: (a) clustering count rate F_{clu}; (b) average number of bubbles per cluster N_{clu}; (c) cluster proportion P_{clu}. Note that only data for $C < 0.3$ (air bubble) and $C > 0.7$ (water droplets) are presented. Legend applies to all figures.

literature, Fig. 5a clearly shows that all probes tested in the present study ($0.25 < Ø_1 < 0.64$ mm and $0.8 < Ø_2 < 1.3$ mm) were able to capture this phenomenon, confirming that the probe's sensor sizes tested within this study gave consistent values.

3.2. Bubble count rate

The bubble count rate data consistently showed a bimodal distribution, with a maximum peak F_{max} in the shear layer region (Fig. 3b), indicating the presence of a strong shear layer within the roller, responsible for breaking large air bubbles into finer pieces [7,33]. A secondary peak occurred near the free-surface (Fig. 3b) at vertical locations where $C = 0.4$–0.6, similarly to self-aerated spillway flows [35]. The occurrence of this secondary peak might be induced by the air entrapment associated with the free-surface fluctuations. The vertical profiles of bubble count rate flattened with increasing longitudinal distance, showing a monotonic decrease of F_{max} with increasing longitudinal distance (Fig. 3b), likely associated with the advection-diffusion

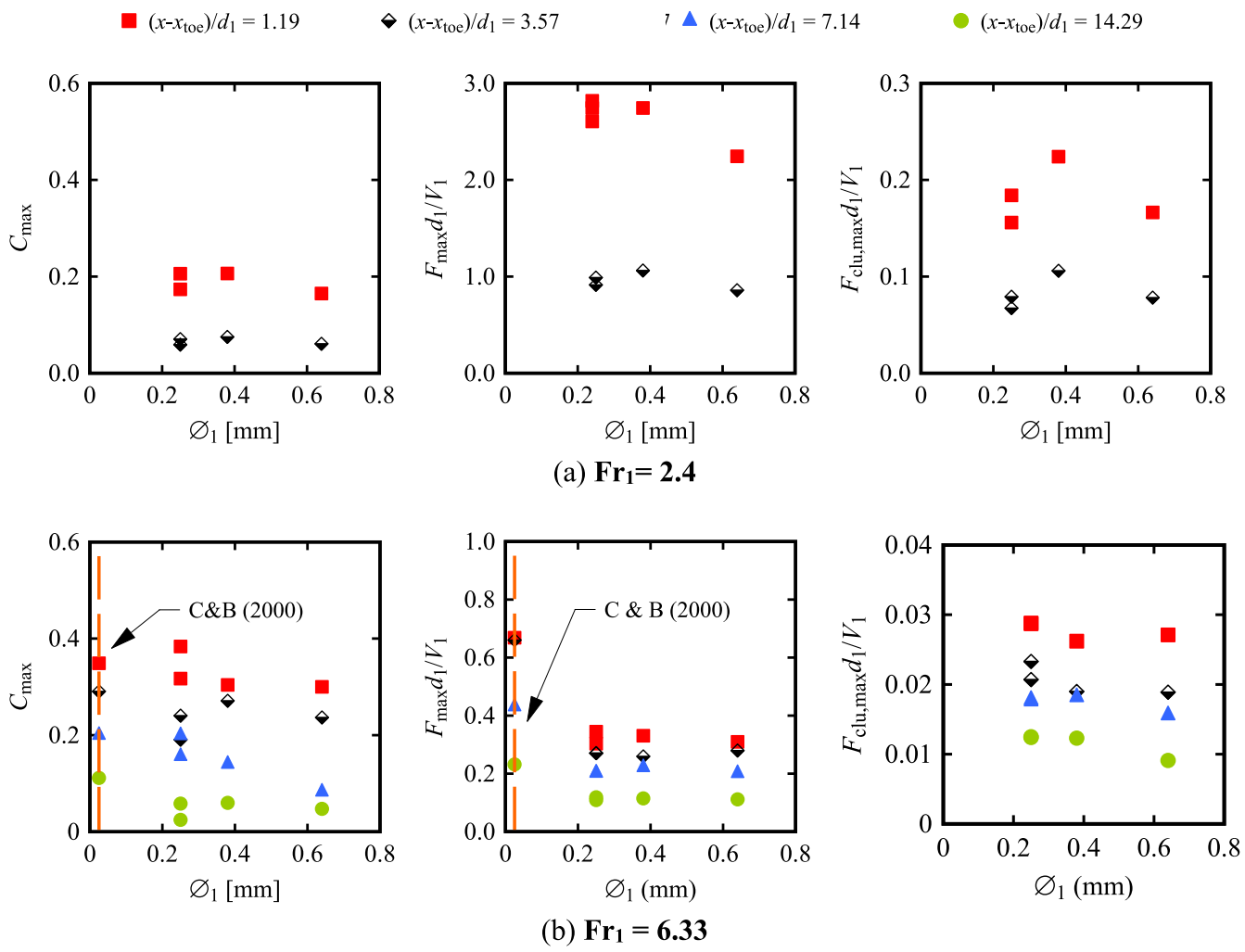

Fig. 5. Maximum values of air-water flow properties for $Fr_1 = 2.4$ (top) and $Fr_1 = 6.33$ (bottom): (left) void fraction; (middle) bubble count rate; (right) clustering count rate. The data for $Fr_1 = 6.33$ were compared to those by Chanson and Brattberg (2000) in Ref. [7] (vertical dashed line).

process within the shear layer.

The bubble count rate profiles measured with probes 1 to 4 (*i.e.* $Ø_1 = 0.25–0.64$ mm) showed results similar in both shape and magnitude. However, the maximum bubble count rate in the shear layer (F_{max}) revealed a slightly decreasing trend for larger probes, with probe 3 ($Ø_1 = 0.64$ mm) detecting 80 % and 86 % of the number of bubbles compared to the probes 1 and 2 ($Ø_1 = 0.25$ mm) at $x_{toe}/d_1 = 1.19$ and 3.57, respectively [18]. In line with these findings, previous data acquired with a finer sensor size ($Ø_1 = 0.025$ mm, [7]), revealed bubble count rates that were almost twice the values obtained with the present thicker probes, thus suggesting that smaller probes are able to capture a substantially larger number of bubbles. This finding is consistent with previous results by Refs. [26,20,23,34,25].

3.3. Interfacial velocities

The distributions of interfacial velocities are presented in Fig. 3c, where the data exhibited positive velocities in the turbulent shear flow. A boundary layer was observed immediately above the channel bed, characterized by increasing velocities until a maximum value is reached, followed by a rapid decrease in the vertical direction. Velocities within the shear layer showed a clear decelerating pattern in the longitudinal direction [*i.e.* for increasing values of $(x\text{-}x_{toe})/d_1$], in line with previous studies. Some flow reversal occurred near the free surface immediately downstream of the roller toe, and quasi-uniform velocity distributions were seen further downstream. At a given location, the velocity distributions derived from the signals acquired with five different probes showed some good agreement. The results implied that, within the tested range, the needle probe sensor's size had a negligible impact on the interfacial velocity measurements.

3.4. Bubble clustering properties

The vertical profile of clustering count rate, *i.e.* the number of clusters per second F_{clu}, exhibited a bimodal distribution in hydraulic jumps for both Froude numbers, with a primary peak $F_{clu,max}$ in the shear layer ($0 < C < 0.3$, air bubbles) and a secondary peak $F_{clu,sec}$ in the recirculation region ($C > 0.7$, water droplets) (Fig. 4a). Note that the secondary peaks of some profiles [*e.g.* $(x\text{-}x_{toe})/d_1 = 1.19$ for $Fr_1 = 2.4$] were absent since the data for $0.3 < C < 0.7$ were not included. The results were consistent with previous studies on hydraulic jumps (*e.g.* Ref. [36]). Similarly to the bubble count rate (F_{max}, Section 3.2), the vertical profiles tended to flatten with increasing longitudinal distance from the roller toe, hence with decreasing values of both $F_{clu,max}$ and $F_{clu,sec}$. In the shear-layer, this longitudinal trend suggested that the advection-diffusion process broke-up clusters, thus reducing their number. In the downstream part of the hydraulic jump roller, the secondary peak became larger than the primary peak, where most clusters

were associated with water droplets near the free surface.

The vertical distributions of the average cluster size, *i.e.* average number of bubbles per cluster N_{clu}, and cluster proportion, *i.e.* the ratio of bubbles in clusters to total bubbles P_{clu}, exhibited comparable profiles to the void fraction, with local maxima located in the lower shear layer region. The one-dimensional clusters consisted of, in average, 2 to 4 air bubbles in the shear layer and 3 to 6 water droplets in the spray region. Away from the roller toe, the clusters tended to be smaller and with a lower bubble proportion.

Interestingly, despite the slightly lower number of bubbles detected by the probe with larger sensors, the comparison for all data, collected with the four probes 0.25 mm $\leq \varnothing_1 \leq$ 0.64 mm, showed similar profiles, indicating negligible effects of the present sensor sizes on the clustering properties in the hydraulic jump with a relatively high Froude number $Fr_1 = 6.3$. Consistently, the distribution of $F_{clu,max}$ in Fig. 5c also shows similar values for all tested probe diameters.

3.5. Bubble chord times

The probability density functions (PDFs) of bubble chord time $(t_{ch})_{air}$ at z_{Fmax} (*i.e.* the elevation where F_{max} occurs) are presented in Fig. 6 at four longitudinal locations behind the roller. PDFs have a bin size of 0.25 ms from 0 to 10 ms and chord time data larger than 10 ms were regrouped, as shown in Fig. 6. All data exhibited similar distributions, with over 70% of the bubbles having a chord time duration of less than 3 ms. It was noted that, with increasing longitudinal distance, the number of smallest (t_{ch}<0.5 ms) and largest (t_{ch}>10 ms) bubbles decreased, which could be associated with a combination of the de-aeration process of larger bubbles and the break-up of larger bubbles during advection.

For a given longitudinal location, the comparison of the chord time data for the four probes showed a good agreement (Fig. 6), suggesting very small effects of inner sensor size within the tested range (0.25 mm $\leq \varnothing_1 \leq$ 0.64 mm).

4. Discussion

The goal of the present study is to present and discuss differences and similarities in the broad range of air-water flow properties measured using four phase-detection needle probes with inner conductors $\varnothing_1$ ranging from 0.25 to 0.64 mm. While the results showed similar values in terms of void fractions and interfacial velocities, the present data showed that the largest probe ($\varnothing_1$ = 0.64 mm) was only able to detect 80–85 % of the bubbles detected with a more widely-used smaller-sensor probe with $\varnothing_1$ = 0.25 mm. This influence of the probe's inner diameter on the bubble count rate is further highlighted when the present data are compared to previous data by Chanson and Brattberg [7], who detected

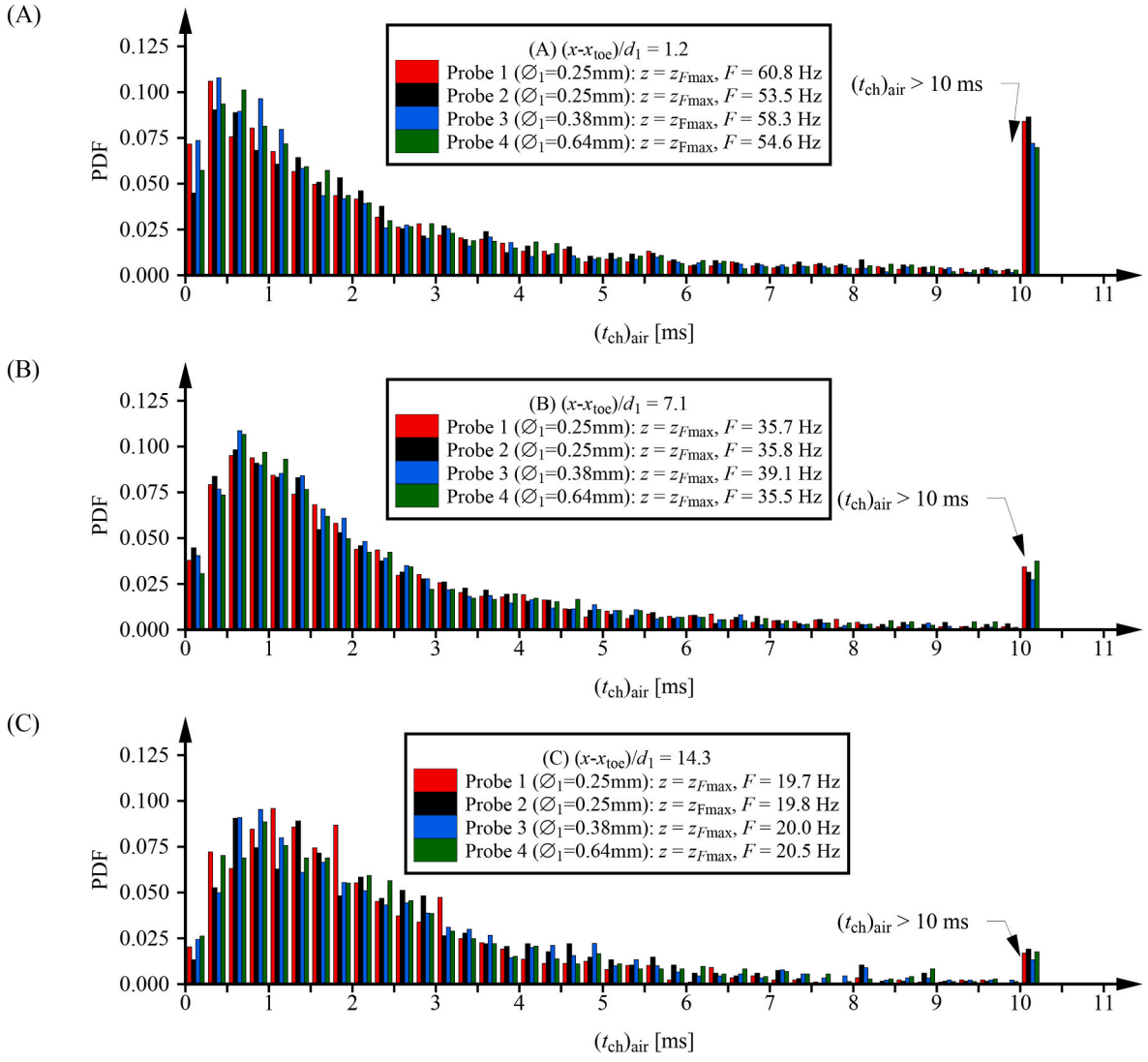

Fig. 6. Probability density functions (PDF) of bubble chord time for hydraulic jump with $Fr_1 = 6.33$ at the characteristic elevation z_{Fmax} (*i.e.* the elevation where F_{max} occurs) at three selected longitudinal positions: (A) $(x - x_{toe})/d_1 = 1.2$; (B) $(x - x_{toe})/d_1 = 7.1$; (C) $(x\text{-}x_{toe})/d_1 = 14.3$.

almost double the bubble frequencies for a hydraulic jump with the same Froude and Reynolds numbers (Fig. 5b). Despite this difference in bubble frequency, the present data revealed similar clustering properties and bubble chord time distributions (Figs. 4 and 6).

This difference in behaviour might be associated with the probe's wetting/drying processes, which allow smaller probe needles to detect finer bubbles. However, the fact that clustering properties and bubble size distributions had similar behaviours, indicates that this difference might be also associated with incomplete piercing processes, as previously suggested by Tang et al. [25] and discussed by Shi et al. [18]. In fact, the current data showed that most differences in the air-water signal were observed at low voltages (*i.e.* in air), which confirms the theory that increasing probe diameters is likely to result in "*sliding-off*" bubble detection. This leads to incomplete voltage drops and therefore in a reduced detection of bubbles. This outcome is in line with earlier results by Refs. [3,37,22,24,38] pointing out a velocity bias due to interactions between bubbles/droplets and the probe tips. This theory is also supported by a new sensitivity analysis, presented in Fig. 7, where values of the maximum bubble count rate F_{max} were computed for different air-water thresholds and normalized with the value $F_{max,50\%}$ obtained for a thresholds of 50% in hydraulic jumps with $Fr_1 = 2.4$ at $(x\text{-}x_{toe})/d_1 = 3.57$. The data showed an increase in the number of bubbles detected by the largest probe for thresholds higher than 60%, compared to the data for smaller probe sensors. This finding suggests that larger probes may require adjusted thresholds in order to detect a similar quantity of air bubbles compared to smaller probes, in line with the approach taken by Bai et al. [16], who utilized an 85% threshold based on laboratory calibration. Alternately, a different signal processing technique might be applied, *e.g.* dual signal threshold, a combination of signal thresholds and gradient thresholds, although the optimum processing technique is yet to be validated. Nonetheless, the disparity linked to the probe sensor size may become particularly pronounced with very large probes, as illustrated by Tang et al. [25] with $Ø_1 = 1$ mm and $Ø_2 = 3$ mm. In this case, adjusting the threshold level proved ineffective in compensating for the difference, necessitating the exploration of alternative strategies.

Overall, the current results show that, for probes up to $Ø_1 = 0.64$ mm and $Ø_2 = 1.3$ mm, the traditional signal processing techniques with a 50 % threshold can be applied to compute the main air-water flow properties with minor errors, while different techniques and methodologies might only be necessary for larger probes, in particular due to an absence of small bubble/droplet detection.

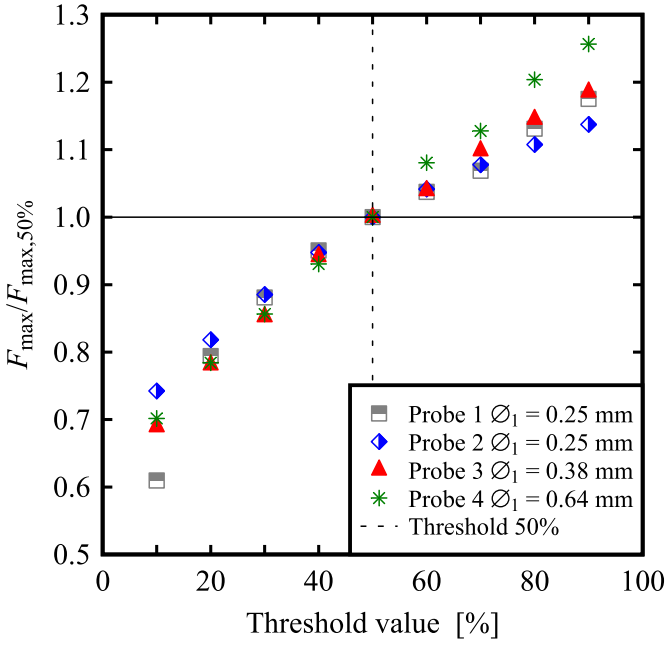

Fig. 7. Sensitivity analysis of the air-water threshold in the computation of the maximum bubble count rate F_{max}, normalized with the value $F_{max,50\%}$ obtained for 50%. Continuous horizontal line represents $F_{max} = F_{max,50\%}$. Hydraulic jump flow conditions: $Fr_1 = 2.4$ at $(x\text{-}x_{toe})/d_1 = 3.57$.

5. Conclusion

New experiments were performed using four dual-tip phase detection probe sensor sizes to characterise a wide range of air-water and bubble clustering properties in hydraulic jumps with low and high Froude numbers, $Fr_1 = 2.41$ and 6.33 respectively. The four needle probes were equipped with different inner sensor diameters $Ø_1$, referred as the inner sensor size, ranging from 0.25 mm to 0.64 mm (Table 1). The two hydraulic jumps exhibited similar flow patterns, featuring a fully breaking roller with air bubble entrainment, large free-surface fluctuations and advection of large-scale coherent structures. This study focused on the air-water flow and bubble characteristics, including clustering properties. The void fraction data exhibited a diffusion process in the breaking roller, with the presence of a local maximum in the developing shear layer. The bubble count rate data showed a bimodal peak distribution, with the primary peak corresponding to the maximum shear force in the developing shear layer, and the secondary peak in the upper part, possibly associated with air entrapment from the free surface fluctuations. The time-averaged interfacial velocity distributions revealed a wall jet, with a recirculation immediately downstream of the roller toe. The cluster count rate data exhibited distributions that were similar to the bubble count rate data, while average cluster size and cluster proportion showed similar behaviours to the void fraction data. The probability density functions (PDFs) of bubble chord times highlighted that the small and large bubbles decreased with increasing longitudinal distance. Overall, air-water properties had features consistent with literature.

The present data comparison showed negligible impacts of the tested sensor sizes ($0.25\text{ mm} < Ø_1 < 0.64\text{ mm}$) on a broad range of air-water flow properties, in terms of the trends, magnitude and maximum values. Some sizeable differences were observed in terms of the bubble count rate, with the larger probes detecting a lesser number of bubbles. This was confirmed through a comparison with the data of Chanson and Brattberg (2002) in Ref. [7] for the same flow conditions ($Fr_1 = 6.33$) and a smaller probe sensor size ($Ø_1 = 0.025$ mm), where the maxima of bubble count rates were almost twice that of the present dataset.

Overall, the current findings suggest that, for probe sensor sizes up to $Ø_1 = 0.64$ mm and $Ø_2 = 1.3$ mm, the traditional signal processing techniques with a 50% threshold can be applied to compute the main air-water flow properties, while different techniques and methodologies might be necessary for larger probes to achieve more '*reliable*' bubble characteristics. Nevertheless, the little difference observed herein between sensor sizes ($0.25\text{ mm} < Ø_1 < 0.64\text{ mm}$) is an encouraging result for the development of sturdier and more robust probes, suitable for field studies and prototype measurements.

Author statement

Rui Shi – Conceptualization, Data curation, Formal Analysis, Methodology, Visualization, Writing – original draft. Davide Wüthrich – Conceptualization, Formal Analysis, Funding acquisition, Methodology, Project administration, Supervision, Visualization, Writing – original draft. Hubert Chanson - Conceptualization, Formal Analysis, Funding acquisition, Methodology, Project administration, Supervision, Writing – review & editing.

Declaration of competing interest

The authors declare that they have no known competing financial interests or personal relationships that could have appeared to influence

the work reported in this paper.

Data availability

Data will be made available on request.

Acknowledgments

The authors would like to thank Dr Hang Wang (Sichuan University, China) and Dr Ivan Stojnic (Stucky, Switzerland) for their helpful comments and suggestions as well as the technical assistance of Jason Van Der Gevel and Stewart Matthews (The University of Queensland). The financial support of the School of Civil Engineering at the University of Queensland, and that of the Swiss National Science Foundation (grant P2ELP2_181794) are acknowledged.

References

[1] N.S.L. Rao, H.E. Kobus, "Characteristics of Self-Aerated Free-Surface Flows." Water and Waste Water/Current Research and Practice, vol. 10, Eric Schmidt Verlag, Berlin, Germany, 1974, p. 224.
[2] I.R. Wood, Air entrainment in free-surface flows, in: IAHR Hydraulic Structures Design Manual No. 4, Hydraulic Design Considerations, Balkema Publ., Rotterdam, The Netherlands, 1991, p. 149.
[3] A. Cartellier, J.L. Achard, Local phase detection probes in fluid/fluid two-phase flows, Rev. Sci. Instrum. 62 (1991) 279–303, https://doi.org/10.1063/1.1142117.
[4] H. Chanson, Air Bubble Entrainment in Free-Surface Turbulent Shear Flows, Academic Press, London, UK, 1997.
[5] L.S. Neal, S.G. Bankoff, A high resolution resistivity probe for determination of local void properties in gas-liquid flows, Am. Inst. Chem. Eng. J. 9 (1963) 49–54, https://doi.org/10.1002/aic.690090415.
[6] Y. Chachereau, H. Chanson, Bubbly flow measurements in hydraulic jumps with small inflow Froude numbers, Int. J. Multiphase Flow 37 (6) (2011) 555–564, https://doi.org/10.1016/j.ijmultiphaseflow.2011.03.012.
[7] H. Chanson, T. Brattberg, Experimental study of the air-water shear flow in a hydraulic jump, Int. J. Multiphase Flow 26 (4) (2000) 583–607, https://doi.org/10.1016/S0301-9322(99)00016-6.
[8] D. Mouaze, F. Murzyn, J.R. Chaplin, Free surface length scale estimation in hydraulic jumps, J. Fluid Eng. 127 (2005) 1191, https://doi.org/10.1115/1.2060736.
[9] H. Wang, Turbulence and air entrainment in hydraulic jumps, Ph.D. Thesis, School of Civil Engineering, The University of Queensland, Brisbane, Australia, 2014, p. 341, https://doi.org/10.14264/uql.2014.542.
[10] D. Wüthrich, R. Shi, H. Chanson, Hydraulic jumps with low inflow Froude numbers: air–water surface patterns and transverse distributions of two-phase flow properties, Environ. Fluid Mech. 22 (2022) 789–818, https://doi.org/10.1007/s10652-022-09854-5.
[11] H. Chanson, Air entrainment in two-dimensional turbulent shear flows with partially developed inflow conditions, Int. J. Multiphase Flow 21 (6) (1995) 1107–1121, https://doi.org/10.1016/0301-9322(95)00048-3.
[12] H. Wang, H. Chanson, Characterisation of transverse turbulent motion in quasi-two-dimensional aerated flow: application of four-point air-water flow measurements in hydraulic jump, Exp. Therm. Fluid Sci. 100 (2019) 222–232, https://doi.org/10.1016/j.expthermflusci.2018.09.004.
[13] B. Hohermuth, R.M. Boes, S. Felder, High-velocity air-water flow measurements in a prototype tunnel chute: scaling of void fraction and interfacial velocity, J. Hydraul. Eng. 147 (11) (2021), 04021044, https://doi.org/10.1061/(ASCE)HY.1943-7900.0001936.
[14] H. Chanson, A Study of Air Entrainment and Aeration Devices on a Spillway Model, Ph.D. thesis, Dept. of Civil Engineering., University of Canterbury, New Zealand, 1988.
[15] P. Cain, I.R. Wood, Instrumentation for aerated flow on spillways, J. Hydraul. Div. ASCE 107 (11) (1981) 1407–1424, https://doi.org/10.1061/JYCEAJ.0005760.
[16] Z. Bai, R. Bai, R. Tang, H. Wang, S. Liu, Case study of prototype hydraulic jump on slope: air entrainment and free-surface measurement, J. Hydraul. Eng. 147 (9) (2021), 05021007, https://doi.org/10.1061/(ASCE)HY.1943-7900.0001916.
[17] H. Wang, R. Tang, Z. Bai, S. Liu, W. Sang, R. Bai, Prototype air-water flow measurements in D-type hydraulic jumps, J. Hydraul. Res. 61 (1) (2023) 145–161, https://doi.org/10.1080/00221686.2022.2132310.
[18] R. Shi, D. Wüthrich, H. Chanson, Discussion of "Performance on intrusive phase-detection probe with large sensor size in air-water flow measurements and application to prototype hydraulic jumps study" by R. Tang, R. Bai and H. Wang, J. Hydraul. Eng. 149 (11) (2023), 07023001, https://doi.org/10.1061/(ASCE)HY.1943-7900.0002022.
[19] T.J. Liu, S.G. Bankoff, Structure of air-water bubbly flow in a vertical pipe - II. Void fraction, bubble velocity and bubble size distribution, Int. J. Heat Mass Transfer 36 (4) (1993) 1061–1072, https://doi.org/10.1016/S0017-9310(05)80290-X.
[20] H. Chanson, L. Toombes, Experimental study of gas-liquid interfacial properties in a stepped cascade flow, Environ. Mech. vol. 2 (2002) 241–263.
[21] H. Chanson, L. Toombes, Experimental investigations of air entrainment in transition and skimming flows down a stepped chute. Application to embankment overflow stepped spillways, in: Research Report No. CE158, Dept. of Civil Engineering, The University of Queensland, Brisbane, Australia, 2001, p. 74.
[22] P.D. Cummings, Aeration Due to Breaking Waves, Dept. of Civil Engrg., University of Queensland, Brisbane, Australia, 1996, p. 523, https://doi.org/10.14264/uql.2015.70.
[23] S. Felder, M. Pfister, Comparative analyses of phase-detective intrusive probes in high-velocity air–water flows, Int. J. Multiphase Flow 90 (2017) 88–101, https://doi.org/10.1016/j.ijmultiphaseflow.2016.12.009.
[24] B. Hohermuth, M. Kramer, S. Felder, D. Valero, Velocity bias in intrusive gas-liquid flow measurements, Nat. Commun. 12 (1) (2021) 4123, https://doi.org/10.1038/s41467-021-24231-4.
[25] R. Tang, R. Bai, H. Wang, Performance of intrusive phase-detection probe with large sensor size in air-water flow measurement and application to prototype hydraulic jump study, J. Hydraul. Eng. 148 (11) (2022), 06022015, https://doi.org/10.1061/(ASCE)HY.1943-7900.0002022.
[26] H. Chanson, C.A. Gonzalez, Physical modelling and scale effects of air-water flows on stepped spillways, J. Zhejiang Univ. - Sci. 6A (3) (2005) 243–250, https://doi.org/10.1007/BF02872325.
[27] C. Gualtieri, H. Chanson, Experimental analysis of Froude number effect on air entrainment in the hydraulic jump, Environ. Fluid Mech. 7 (2007) 217–238, https://doi.org/10.1007/s10652-006-9016-1.
[28] H. Chanson, Air-water flow measurements with intrusive, phase-detection probes: can we improve their interpretation? J. Hydraul. Eng. 128 (2002) 252–255, https://doi.org/10.1061/(ASCE)0733-9429.
[29] C. Crowe, M. Sommerfield, Y. Tsuji, Multiphase Flows with Droplets and Particles, CRC Press, Boca Raton, USA, 1998, p. 471.
[30] K.J. Sene, J.C.R. Hunt, N.H. Thomas, The role of coherent structures in bubble transport by turbulent shear flows, J. Fluid Mech. 259 (1994) 219–240, https://doi.org/10.1017/S0022112094000108.
[31] H. Chanson, G. Carosi, Turbulent time and length scale measurements in high-velocity open channel flows, Exp. Fluid 42 (3) (2007) 385–401, https://doi.org/10.1007/s00348-006-0246-2.
[32] H. Chanson, S. Aoki, A. Hoque, Bubble entrainment and dispersion in plunging jet flows: freshwater versus seawater, J. Coast Res. 22 (3) (2006) 664–677, https://doi.org/10.2112/03-0112.1.
[33] H. Wang, Z. Hu, H. Chanson, Two-dimensional bubble clustering in hydraulic jumps, Exp. Therm. Fluid Sci. 68 (2015) 711–721, https://doi.org/10.1016/j.expthermflusci.2015.07.006.
[34] F. Murzyn, D. Mouaze, J.R. Chaplin, Optical fibre probe measurements of bubbly flow in hydraulic jumps, Int. J. Multiphase Flow 31 (1) (2005) 141–154, https://doi.org/10.1016/j.ijmultiphaseflow.2004.09.004.
[35] H. Chanson, L. Toombes, Air-water flows down stepped chutes: turbulence and flow structure observations, Int. J. Multiphase Flow 28 (2002) 1737–1761, https://doi.org/10.1016/S0301-9322(02)00089-7.
[36] H. Chanson, Y. Chachereau, Scale effects affecting two-phase flow properties in hydraulic jump with small inflow Froude number, Exp. Therm. Fluid Sci. 45 (2013) 234–242, https://doi.org/10.1016/j.expthermflusci.2012.11.014.
[37] A. Cartellier, E. Barrau, Monofiber optical probes for gas detection and gas velocity measurements: conical probes, Int. J. Multiphase Flow 24 (8) (1998) 1265–1294, https://doi.org/10.1016/S0301-9322(98)00032-9.
[38] A. Serizawa, I. Kataoka, I. Michiyoshi, Turbulence structure of air-water bubbly flows - I. Measuring techniques, Int. J. Multiphase Flow 2 (3) (1975) 221–233, https://doi.org/10.1016/0301-9322(75)90011-7.